A&A 462, 1121–1126 (2007)
DOI: 10.1051/0004-6361:20065888

Astronomy & Astrophysics

Magnetic properties of flare-CME productive active regions and CME speed⋆ *(Research Note)*

J. Guo[1], H. Q. Zhang[1], and O. V. Chumak[2]

[1] National Astronomical Observatories, Chinese Academy of Sciences, Beijing 100012, PR China
e-mail: guojuan@bao.ac.cn
[2] Sternberg Astronomical Institute (SAI), Moscow State University, Moscow 119899, Russia

Received 23 June 2006 / Accepted 17 September 2006

ABSTRACT

Aims. We study the properties of magnetic field of flare-coronal-mass-ejection (flare-CME) productive active regions and their statistic correlations with CME speed.
Methods. We used a sample of 86 flare-CMEs in 55 solar active regions. Four measures, including the tilt angle (*Tilt*), total flux (*Ft*), length of the strong-field and strong-gradient main neutral line (*Lsg*) and effective distance (d_E), are used to quantify the properties of the magnetic field of flare-CME productive active regions.
Results. The results are as follows: (1) for CMEs initiating in active regions, fast CMEs tend to initiate in active regions with large *Ft* or large d_E. (2) In flare-associated CMEs, faster CMEs tend to be accompanied by more intense flares. (3) The parameters d_E, *Lsg* and *Ft* correlate well with one another, especially *Ft* and *Lsg*. (4) The occurrence of 11 slow CMEs and 1 fast CME in β type regions with *Lsg* far below the threshold reminds us of some exceptions to be considered when *Lsg* with the threshold is used to predict the CME productivity of active regions.

Key words. Sun: activity – Sun: magnetic fields – Sun: coronal mass ejections (CMEs) – Sun: flares

1. Introduction

Solar coronal mass ejections (CMEs) are the most spectacular form of solar activity. Each CME can carry a mass of up to 10^{13} kg and release up to 10^{25} J of energy from the Sun into the heliosphere. Fast halo CMEs in particular drive hazardous space weather in the form of intense solar energetic particle events and severe geomagnetic storms. Since most CMEs initiate in active regions (Subramanian & Dere 2001), it is important to understand what kinds of active regions will produce fast CME. This knowledge is a great help for predicting space weather.

From observations of the magnetic structure of active regions, it was noticed long ago that CME productive active regions are likely to show overall non-potential field configurations of a characteristic form (Moore & LaBonte 1980; Moore et al. 1997, 2001; Canfield et al. 1999). Measurements of the global non-potentiality of an active region can be obtained from a vector magnetogram of the region regardless of the chirality of global magnetic shear or twist in chromospheric or coronal images (Falconer et al. 1997, 2001). However, the analysis of vector magnetograms has experienced difficulties even as new instruments have been developed. The most notable ones are calibration, resolution of 180 degree ambiguity and correction of the projection effect when the region is not close to the solar disk center. Relative to vector magnetograms, conventional magnetograms are simpler and more robust and have proved they can monitor solar magnetic fields continuously and uniformly over many years. It is desirable to find measures that can be obtained directly from line-of-sight magnetograms and that may represent the non-potentiality of active regions.

Zhang (2001, 2006) studied NOAA 6659 and found that the shear and gradient of the magnetic field are important and that both reflect a part of the electric current in solar active regions, which is notable in the vicinity of the magnetic neutral line. From a sample of 17 vector magnetograms, Falconer et al. (2003) found that the length of the strong-field and strong-gradient main neutral line (*Lsg*) is a viable proxy for the overall non-potentiality of active regions that can be measured from longitudinal magnetograms. Hahn et al. (2005) studied co-registered photospheric vector magnetograms and chromospheric Hα images for 29 flares and found that flares tend to originate in regions of a high twist gradient and lie close to chirality inversion lines.

After a detailed comparison of gradient and shear in 5 well-known active regions that produced strong flares, Wang et al. (2006) found that the magnetic gradient could even be a better proxy to predict where a major flare might occur than is the magnetic shear. Because the gradient can be measured from a longitudinal magnetogram obtained from conventional magnetographs, it is a dependable substitute for magnetic shear for use in operational CME forecasting. However, no study has been carried out to analyze the correlation between the *Lsg* of CME productive active regions and CME speed (V_{CME}).

In our recent work (Guo et al. 2006), we revealed that effective distance (d_E), a structural parameter proposed by Chumak & Chumak (1987), could roughly quantify the magnetic complexity of active regions and consequently be useful in studying the quantitative evolution of the magnetic complexity of active

⋆ Table 1 is only available in electronic form at
http://www.aanda.org

regions and the quantitative relationship between the magnetic complexity and activity of active regions. We found there is a basic agreement between $d_{\rm E}$ and the Mount Wilson magnetic classification (MWMC). For example, active regions with β configuration usually show $d_{\rm E}$ below unity, while active regions with δ configuration, the most notable indicator of non-potentiality, usually show $d_{\rm E}$ above unity. The value of $d_{\rm E}$ increases in the developing δ structure, the value of $d_{\rm E}$ decreases in the decaying δ structure and the value of $d_{\rm E}$ changes insignificantly in stable magnetic configurations. As a pilot study, we also studied 43 flare-associated and 25 CME-associated active regions and found that $d_{\rm E}$ correlates with flare index and $V_{\rm CME}$ better than total flux (Ft) and Tilt angle ($Tilt$).

In the present work, we focus on the flare-CME productive active regions and expand the previous sample into a larger one, which is composed of 86 flare-CMEs initiating in 55 active regions near the central meridian. The new sample includes most of the important flare-CMEs initiating in active regions in the interval from 1997 to 2005. A parameter Lsg is added to the parameter set. We also study the relationship among the four parameters and the relationship between $V_{\rm CME}$ and the CME-associated flare intensity. The paper will be arranged as follows. In Sect. 2, we introduce the data and procedure used. Our analysis of one example and the statistical results are given in Sect. 3. The summary is given in Sect. 4.

2. Data and procedure

To measure the parameters of flare-CME productive active regions accurately, we only chose the events whose source origins were located within ±45° of the central meridian. From the CMEs studied by Tian et al. (2003), Zhou et al. (2003) and Moon et al. (2005), those satisfying the above selection criteria were included. We also referred to the SEC Solar Event Weekly Report at `http://www.sec.noaa.gov/weekly/index.html` and the SOHO/LASCO CME catalogs at `http://cdaw.gsfc.nasa.gov/CME_list/index.html` to identify the association of some flare-CMEs with active regions. We finally collected 86 CMEs, which originated in 55 active regions near the central meridian. Then full disk magnetograms with a 96-min cadence taken by *SOHO/MDI* were used to get longitudinal magnetograms of flare-CME productive active regions. We required the full-disk magnetograms for at least 25 min and at most 96+25 min prior to the flare onset. We did not use magnetograms obtained closer to the flare onsets because impulsive variations in the magnetic helicity change rate were sometimes associated with flares. This magnetic helicity changes peaked within ±20 min of the X-ray flares' peak time in all the events they studied (Moon et al. 2002). For example, if a flare onset was at exactly the time one magnetogram was taken or within 25 min after one magnetogram was taken, we used the preceding magnetogram.

The nonlinear mapping, flux density interpolation and the geometrical forecasting correction were all done following the method by Chae et al. (2001). Thus for each longitudinal magnetogram of the CME-associated active region, the effect of solar differential rotation were removed and the vertical field strength became equal to the line-of-sight field strength times $1/\cos\psi$, where ψ is the heliocentric angle of the region (Liu & Zhang 2006). We finally get a sample of 86 longitudinal magnetograms of CME-associated active regions. In order to exclude the effect of noise and to keep important weak fields (e.g. newly emerging or decaying regions), 100 Gauss was chosen as the threshold for MDI full-disk magnetograms in our measurement of the former three parameters, which we describe bellow.

We introduce 4 parameters employed as following:

(1) Ft, the total flux of an active region, is a quantitative measure of an active region's size, which is well correlated with its overall productivity for energetic events (Giovanelli 1939; McIntosh 1990; Canfield et al. 1999; Tian et al. 2002).

(2) *Tilt* is defined as the angle between the direction of the polarity axis of an active region and the local latitude, which could be computed with the equation $\tan(Tilt) = \delta y/\delta x$, where δx and δy are Cartesian coordinate differences between the leading and following polarities of an active region in the heliographic plane. This definition of tilt is similar to the one used by Tian et al. (2001). The *Tilt* of solar active regions relates to the writhe (spatial deformation or turning of the axis) of the flux tube, which is one of the measurable parameters of solar active regions that give us information about subsurface physical processes associated with the creation and subsequent evolution of magnetic flux tubes inside the Sun (Holder et al. 2004).

(3) $d_{\rm E}$, effective distance, is a structural parameter proposed by Chumak & Chumak (1987). This parameter is defined as ($d_{\rm E} = (R{\rm n} + R{\rm s})/R{\rm sn}$), where $R{\rm s} = (N{\rm s}/\pi)^{-1/2}$, $R{\rm n} = (N{\rm n}/\pi)^{-1/2}$, $N{\rm s}(N{\rm n})$ is total area of the negative (positive) polarity, $R{\rm s}(R{\rm n})$ is the equivalent radius of negative (positive) polarity and $R{\rm sn}$ is the distance between the flux-weighted centers of opposite polarities. This parameter could roughly quantify the magnetic complexity of active regions, which makes it possible to study the quantitative evolution of the magnetic complexity of active regions and the quantitative relationship between magnetic complexity and the activity of active regions. Our recent work (Guo et al. 2006) confirmed that there is a basic agreement between $d_{\rm E}$ and MWMC. For example, active regions with β configuration usually show $d_{\rm E}$ below unity, while active regions with δ configuration, the most notable indicator of non-potentiality, usually show $d_{\rm E}$ above unity. The value of $d_{\rm E}$ increases in the developing δ structure, the value of $d_{\rm E}$ decreases in the decaying δ structure and the value of $d_{\rm E}$ changes insignificantly in stable magnetic configurations. In addition, $d_{\rm E}$ correlates better with flare index and $V_{\rm CME}$ than do Ft and $Tilt$.

(4) Lsg, the length of the portion of the main neutral line on which the potential transverse field is strong (>150 G) and the horizontal gradient of the longitudinal magnetic field is sufficiently steep (>50 G/Mm) (Falconer et al. 2003). The neutral line separates opposite polarities of the longitudinal magnetic field. High gradient and strong shear usually appear in the vicinities of neutral lines, where flares frequently occur (Zirin & Liggett 1987; Zirin 1988; Hagyard & Rabin 1986; Hagyard 1988; Zhang et al. 1994; Zhang 2001). Lsg is a measure of active region non-potentiality that can be measured from a longitudinal magnetogram. Falconer et al. (2003) found that Lsg correlated with CME productivity of active region strongly and was useful in operational CME forecasting. They also defined a threshold of 36 000 km (about 50 arcsec) for Lsg of active regions for the occurrence of CMEs. To measure Lsg, the first step is to determine the location of the neutral line from the change in sign of the line-of-sight magnetograms. The strong-field and strong-gradient main neutral line is then determined for the pixels that touch the neutral line and have a potential transverse field greater than 150 G and gradient greater than 50 G/Mm. When some segment of the "neutral lines" (the group of

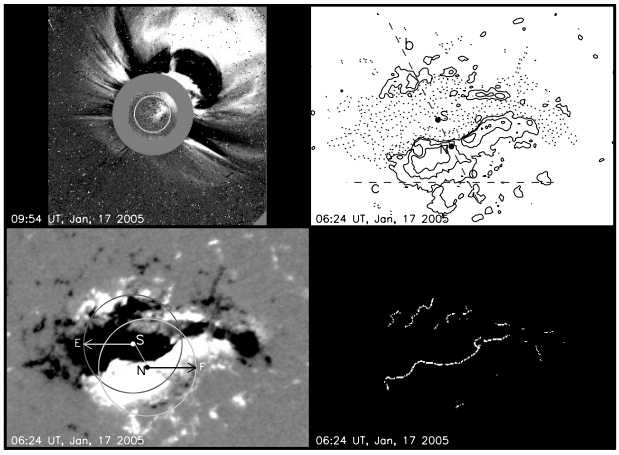

Fig. 1. *Top left*: a complex NW-directed full-halo CME initiating in NOAA 10720 and obtained by LASCO/C2 at 09:54 on Jan. 17, 2005. *Top right*: the longitudinal field with contour levels of 100, 500, 1000 Gauss. The angle b-o-c is the tilt angle for this magnetogram, about 58.06°. *Bottom left*: a sketch of d_E for this magnetogram (d_E = 3.55). The circle with a center at "N" ("S") represents the positive (negative) polarity. The line S-N is the distance between the flux-weighted centers of opposite polarities. The line with an arrow S-E (N-F) is the equivalent radius of negative (positive) polarity. *Bottom right*: the strong-field and strong-gradient main neutral line. Note the last three panels are for NOAA 10720 at 06:24 UT with a field of view of 338″ × 242″. The spot marked with "S" ("N") indicates the flux-weighted center of negative (positive) polarity in the *Top right* and *Bottom left panels*.

pixels selected above) is more than one pixel wide, some pixels of this segment are removed to make that part of neutral line one pixel wide. Then *Lsg* is estimated from both the pixel size and the number of pixels bracketing the strong-field and strong-gradient portions of the main neutral line. Here arcsec is chosen as the unit of *Lsg*.

3. Results

3.1. Results of one example

As an example, in Fig. 1 we present a typical data set that we have compiled for a CME-productive active region NOAA 10720. According to the SEC Solar Event Weekly Report, this region produced an X3.8 flare on Jan. 17, 2005. The flare started at 06:59, reached maximum at 09:52 and ended at 10:07. Associated with this flare, a complex NW-directed full-halo CME at a speed of 2547 km s^{-1} appeared at C2 at about 09:54 (the top left panel in Fig. 1), so we choose longitudinal magnetograms of NOAA 10720 at 06:24, about 35 min prior to the flare onset, to measure the 4 parameters. *Tilt* and d_E of this magnetogram are sketched in the top right panel and bottom left panel in Fig. 1, respectively. Calculating both of them relates to flux-weighted centers of two polarities. "S" indicates the flux-weighted center of negative polarity and "N" indicates the flux-weighted center of positive polarity. For *Tilt*, b-o joins the flux-weighted centers "S" and "N", c-o is a parallel line of the local latitude, and the angle b-o-c is the tilt angle for this magnetogram. It is about 58.06°. For d_E, the cycle with a center at "S" and with the same area as the negative polarity represents the photosphere cross section of the flux rope of negative polarity, and the cycle with a center at "N" and with the same area as the positive polarity represents the photosphere cross section of the flux rope of positive polarity. The two simplified polarities are located so close to each other that they largely overlap each other. This geometric representation could be regarded as a sketch map of the δ configuration, which is defined as the umbra of opposite polarity lying in a common penumbra. By calculating the ratio of the sum of radii of two opposite polarities to the distance between the flux-weighted centers of the two opposite polarities, d_E could roughly quantify the magnetic configuration of this active region. For this magnetogram, d_E is 3.55 (by comparison, most of β type regions show d_E less than unity in Table 1), which indicates that the non-potentiality of this region is great. In the bottom right panel of Fig. 1, we show gradient on the main neutral line on which the potential transverse field is strong (>150 G) and the gradient of the line-of-sight field is sufficiently steep (>50 G/Mm). The parameter *Lsg* is the length of the main neutral line. For this image, *Lsg* is 523 arcsec, which is much longer than the threshold of 50 arcsec.

3.2. Statistical results

The physical characteristics of 86 CMEs and properties of a longitudinal magnetic field of CME-productive active regions are summarized in Table 1. In this section, we examine the agreement between d_E and MWMC and the reliability of *Lsg* on the threshold in predicting active region CME productivity. We study the correlations among the four parameters, the relationships between the four parameters and the CME speed and the relationship between CME speed and the flare intensity.

3.2.1. Examination of the agreement between d_E and MWMC

First, to examine the basic agreement between d_E and MWMC, we analyzed d_E of 55 CME-productive active regions shown in Table 1. Some active regions are counted several times as they show different magnetic classes at different times. For example, NOAA 8210 was a $\beta\gamma$ type region on April 29, a $\gamma\delta$ type region on May 1 and a $\beta\gamma\delta$ type on May 2. This means that this region was counted 3 times as 3 types. We find that most (20/24) β regions show d_E less than unity. Both of the 2 $\beta\delta$ regions, the only $\gamma\delta$ region and most (18/20) $\beta\gamma\delta$ regions show d_E above unity. For the 14 $\beta\gamma$ regions, there are some discrepancies: 6 regions show d_E above unity, while 8 regions show d_E below unity. These results are consistent with our previous work (Guo et al. 2006), in which 24 active regions of different types were analyzed. With more samples, the present results confirm there is a basic agreement between d_E and MWMC, especially for active regions of β and δ structure.

3.2.2. Reliability of *Lsg* on the threshold in predicting active region CME productivity

From Table 1, we find that most (74/86) CMEs occurred with *Lsg* above the threshold of 50 arcsec, which confirms that *Lsg* with the threshold is statistically well correlated with the CME productivity of active regions. However, it also should be noticed that 12 CMEs occurred with *Lsg* far below the threshold and 4 CMEs even occurred with *Lsg* being 0. These remind us that there are still some unexpected cases to be considered when *Lsg* with the threshold is used to predict the CME productivity of active regions. In addition, all the 12 unexpected CMEs initiate in active regions with β type configuration and most (11/12) are slow CMEs with a speed less than 1000 km s^{-1}.

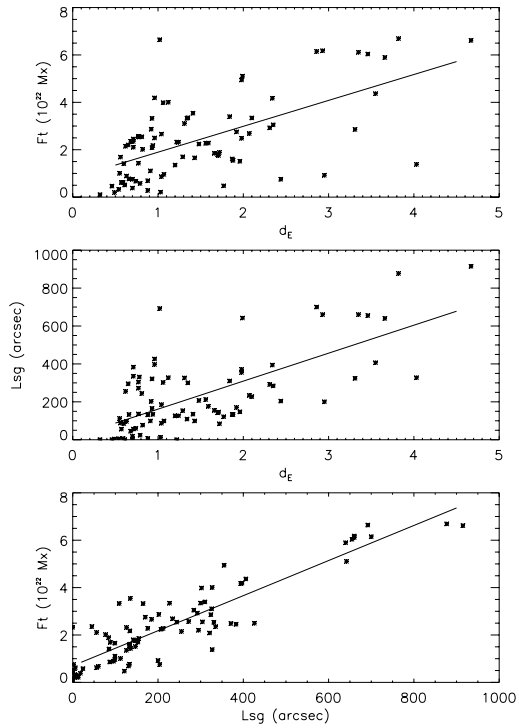

Fig. 2. *Top*: d_E vs. Ft for the 86 CMEs. The solid line denotes a least-square quadratic polynomial fit to the data points. *Middle*: same as the top panel, but for d_E vs. Lsg. *Bottom*: same as the top panel, but for Lsg vs. Ft.

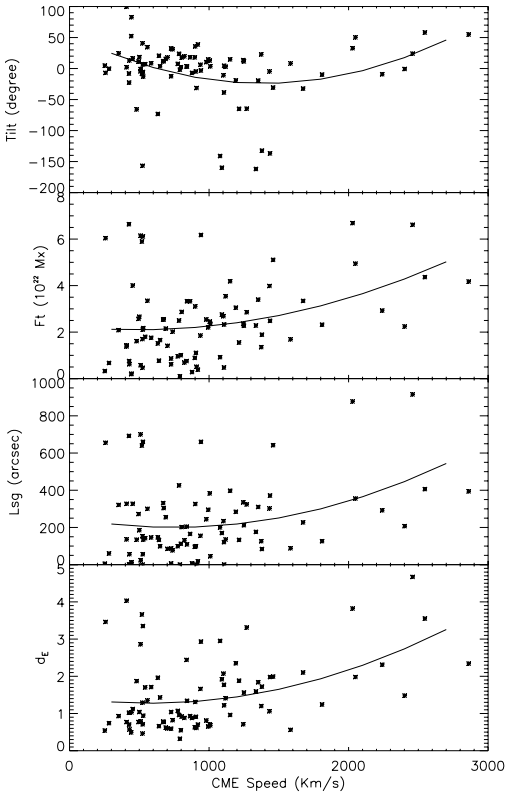

Fig. 3. *Top*: V_{CME} vs. *Tilt* for the 86 CMEs. The solid line denotes a least-square quadratic polynomial fit to the data points. The *second panel*: same as the top panel, but for V_{CME} vs. Ft. The *third panel*: same as the top panel, but for V_{CME} vs. Lsg. *Bottom*: same as the top panel, but for V_{CME} vs. d_E.

3.2.3. Correlations among the four parameters

It is worth paying attention to the correlations among the 4 parameters. We present some correlations among Ft, d_E and Lsg in Fig. 2. For each relationship, we estimate Pearson's linear correlation coefficient (CC_{Pl}) and Spearman's rank correlation coefficient (CC_{Sr}) with its two-sided significance (S_{Sr}) for its deviation from zero. Note a low value of S_{Sr} indicates a significant Spearman's rank correlation. The coefficients for the relationships in Fig. 2 are summarized in Table 2, from where one may find that the three parameters Ft, d_E and Lsg correlate well with one another, especially Ft and Lsg.

Physical speaking, active regions with opposite polarities located near each other tend to show large d_E and a steep magnetic gradient, for example δ type regions. The length of the strong field and strong gradient on the main neutral line is Lsg, so it is reasonable that d_E and Lsg correlate with each other well in describing the overall non-potentiality of the magnetic field of active regions. Statistically active regions with large flux are likely to show large d_E and large Lsg because the separation between opposite polarities is not unlimited. In addition, active regions with large d_E, large Lsg and large Ft are likely to produce several intensive flare and very fast CMEs, for example NOAA 10486, NOAA 9415, NOAA 9077 and NOAA 10720 in Table 1.

We also examined the correlations between *Tilt* and the three other parameters, but we failed to obtain good results. However, we note that, among the 31 fast CMEs in Table 1, 17 fast CMEs initiated in 10 active regions with negative *Tilt*. These active regions with very turned axis of the flux tube show complex configurations (large d_E and large Lsg). There are still some active regions whose magnetic configurations are so complex that it is unable to locate their predominant polarities or the direction of tilt angle, for example NOAA 10486. For such active regions, *Tilt* may have been ambiguously measured and the other three parameters seem to be more viable for predicting of flare-CMEs activity. In fact, NOAA 10486 shows large Ft, large d_E and large Lsg, which indicates that this region is severe flare-CME productive. During the period from October 22 to November 4, when the region passed through the solar disk, 7 X-class flares, including the biggest solar flare (X28) seen in recent years, 19 M-class flares and 8 fast CMEs occurred in NOAA 10486.

In summary, studying active regions synthetically with many parameters could lead to efficient prediction of severe solar activities.

Table 2. Correlation among the parameters.

	CC_{Pl}	CC_{Sr}	S_{Sr}
d_E vs. Ft	0.6180	0.5690	1.09e-8
d_E vs. Lsg	0.6885	0.6088	5.0e-10
Ft vs. Lsg	0.8971	0.8209	3.8e-22

3.2.4. Four parameters vs. V_{CME}

We show the speed of 86 CMEs versus the 4 parameters of magnetograms of CME-associated active regions in Fig. 3. The estimated correlation coefficients corresponding to the relationships are shown in Table 3. It is found that, although the estimated Pearson's linear correlation coefficients between d_E and V_{CME}, Ft and V_{CME} decrease a bit compared to the results of Guo et al. (2006), the correlation is still there: d_E correlate better with V_{CME} than *Tilt* and Ft. Furthermore, it should be noticed that the correlation coefficient of Ft vs. CME speed is affected less by the number of the sample.

Table 3. $V_{\rm CME}$ and the parameters.

	$CC_{\rm Pl}$	$CC_{\rm Sr}$	$S_{\rm Sr}$	$CC_{\rm P}$
$V_{\rm CME}$ vs. *Tilt*	−0.0406	−0.1256	0.2491	
$V_{\rm CME}$ vs. Ft	0.3337	0.3386	0.0014	0.1290 ($d_{\rm E}$) 0.1752 (Lsg)
$V_{\rm CME}$ vs. Lsg	0.289	0.2370	0.0280	−0.0239 (Ft) 0.0325 ($d_{\rm E}$)
$V_{\rm CME}$ vs. $d_{\rm E}$	0.3888	0.3499	9.6e-4	0.2463 (Ft) 0.2730 (Lsg)

We notice that $d_{\rm E}$ correlates much better with $V_{\rm CME}$ than Lsg, though they correlate with each other well for describing the overall non-potentiality of the magnetic field of active regions. This may be because Lsg and $d_{\rm E}$ respect the overall magnetic non-potentiality of active regions from different aspects. $d_{\rm E}$ describes the overall complexity of magnetic configuration of active regions and there is basic agreement between $d_{\rm E}$ and MWMC. Active regions with high $d_{\rm E}$ usually show δ configuration, which is the most notice indicator of the non-potentiality of active regions. From Table 1, we can find there are 31 fast CMEs: 18 fast CMEs from $\beta\gamma\delta$ regions, 8 fast CMEs from $\beta\gamma$ regions, 2 fast CMEs from $\beta\delta$ regions and only 3 fast CMEs from simple β regions. In contrast, there is no obvious correlation between Lsg and the magnetic classification of active regions, although Lsg is strongly correlated with the CME-productivity of active regions (Falconer et al. 2003).

The Spearman's rank correlation coefficients of $V_{\rm CME}$ with the four parameters almost have equivalent values to the corresponding Pearson's linear correlation coefficients, while their two-sided significance levels are very different from one another. Among the four relationships, the correlation between CME speed and $d_{\rm E}$ shows the low value for the two-sided significance, which indicates the corresponding Spearman's rank correlation is the most significant.

Because the three parameters Ft, Lsg and $d_{\rm E}$, correlate with one another well (Sect. 3.2.3), $V_{\rm CME}$ may be dependent on all three magnetic quantities. It is not apparent whether the above dependence of $V_{\rm CME}$ on either Lsg and $d_{\rm E}$ is due to the interdependence of Lsg and $d_{\rm E}$ on Flux Ft. If it is due to this interdependence, then the $V_{\rm CME}$ versus $d_{\rm E}$ and Lsg correlations recovered in this paper are meaningless. To effectively remove the interdependence of $V_{\rm CME}$, $d_{\rm E}$, Lsg and Ft, we did an analysis involving the partial correlation coefficient ($CC_{\rm P}$), which explored the relationship between two quantities while holding a third quantity constant. For example, we generated the partial correlation between $V_{\rm CME}$ and $d_{\rm E}$, while holding Ft constant, and repeated this for $V_{\rm CME}$ and Lsg, while holding Ft constant. In the column of $CC_{\rm P}$ (see the last column in Table 3), the bracketed parameter indicates the parameter held as constant when the $CC_{\rm P}$ is analyzed. It was found that the partial correlation coefficients between $V_{\rm CME}$ and Ft (holding Lsg or $d_{\rm E}$ constant, respectively), $V_{\rm CME}$ and $d_{\rm E}$ (holding Lsg or Ft constant, respectively), decreased a bit compared to the corresponding Pearson's linear or Spearman's rank correlation coefficients, which confirms that there are correlations between $V_{\rm CME}$ and Ft, $V_{\rm CME}$ and $d_{\rm E}$. However, the partial correlation coefficients between $V_{\rm CME}$ and Lsg (when holding Ft or $d_{\rm E}$ constant, respectively) are very small compared to the corresponding Pearson's linear or Spearman's rank correlation coefficients, which indicates that there is no true correlation between $V_{\rm CME}$ and Lsg and the apparent correlation is due to their interdependence on Ft or $d_{\rm E}$.

In the light of the above discussions, we conclude that for CMEs initiating in active regions, fast CMEs tend to initiate in active regions with large Ft or large $d_{\rm E}$. Although the correlation coefficients are not strong, the small two-sided significance values and the partial correlation coefficient confirm the above trend.

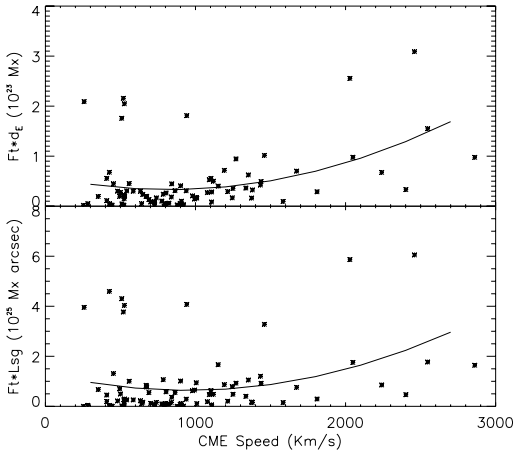

Fig. 4. *Top*: $V_{\rm CME}$ vs. $Ft \times d_{\rm E}$ for the 86 CMEs. The solid line denotes a least-square quadratic polynomial fit to the data points. *Bottom*: same as the top panel, but for $V_{\rm CME}$ vs. $Ft \times Lsg$.

Table 4. $V_{\rm CME}$ and combined parameters.

	$CC_{\rm Pl}$	$CC_{\rm Sr}$	$S_{\rm Sr}$
$V_{\rm CME}$ vs. $Ft \times d_{\rm E}$	0.3665	0.3815	2.9e−4
$V_{\rm CME}$ vs. $Ft \times Lsg$	0.2495	0.2842	0.0080

It is generally believed that the strength of magnetic field and the complexity of the magnetic configuration prior to the eruption determine which type of CMEs the region is able to expel. The increase in the stress in the source region is the crucial factor, while the strength of the field determines how much free energy can be stored in it (Schmieder 2005). In the present paper, both $d_{\rm E}$ and Lsg quantify the overall non-potentiality of the magnetic field of active regions and then relate to the stress in the source region. The value of Ft quantifies the strength of an active region, which provides a clue to the energy available for major solar events. It is reasonable to expect that active regions with a large Ft (strong magnetic field) and large $d_{\rm E}$ or Lsg (high complexity or high overall non-potentiality) might produce fast CMEs.

For the 86 events, we examined the correlations between $V_{\rm CME}$ and two combined parameters, $Ft \times d_{\rm E}$ and $Ft \times Lsg$ (Fig. 4). From Table 4, it is found that any kind of correlation coefficient between CME speed and $Ft \times d_{\rm E}$ is better than it is between $V_{\rm CME}$ and $Ft \times Lsg$. However, the correlation between $V_{\rm CME}$ and either of the two combined parameter is not as good as that we expected. After detailed analysis we find it is due to the appearance of six events: five slow CMEs from NOAA 9393, a huge active region with very strong magnetic field (large Ft) and a very complex magnetic configuration (large Lsg and large $d_{\rm E}$), and one slow CME from NOAA 8674, a region with large Ft and large Lsg. Without the six events, the correlation quantities between $V_{\rm CME}$ and two combined parameters will be $CC_{\rm Pl} = 0.6557$, $CC_{\rm Sr} = 0.5613$ with $S_{\rm Sr} = 6.11\text{e}{-8}$ for $Ft \times d_{\rm E}$ and $CC_{\rm Pl} = 0.5520$, $CC_{\rm Sr} = 0.4565$ with $S_{\rm Sr} = 2.08\text{e}{-5}$ for $Ft \times Lsg$. It should be noticed that $Ft \times d_{\rm E}$ correlates better with $V_{\rm CME}$ than $Ft \times Lsg$ either with or without the six special events. These indicate that active regions with large Ft and large $d_{\rm E}$ tend to produce faster CMEs, than do active regions with large Ft and large Lsg.

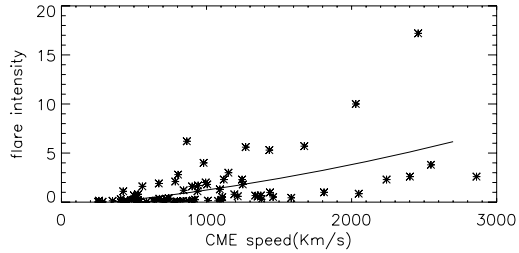

Fig. 5. $V_{\rm CME}$ vs. flare intensity for the 86 CMEs and the 86 accompanied flares. The solid line denotes a least-square quadratic polynomial fit to the data points.

Table 5. $V_{\rm CME}$ and flare intensity.

	$CC_{\rm Pl}$	$CC_{\rm Sr}$	$S_{\rm Sr}$
$V_{\rm CME}$ vs. $I_{\rm flare}$	0.5777	0.6462	1.83e−11

3.2.5. $V_{\rm CME}$ vs. flare intensity

We notice that among the 86 CMEs, 31 are fast CMEs with a speed of more than 1000 km s^{-1}. All the fast CMEs are accompanied by X-ray flares such as M and X class flares. For further examination of the correlation between CMEs and flares, we show the speed of 86 CMEs versus GOES X-ray peak flux of the accompanied flares in Fig. 5, where a C1 flare is counted as 0.01, an M2 flare is counted as 0.2, an X1 flare is counted as 1, and so on.

From Table 5, it is found that there is relatively good correlation between $V_{\rm CME}$ and flare intensity ($I_{\rm flare}$). The estimated correlation coefficients are $CC_{\rm Pl} = 0.5777$ and $CC_{\rm Sr} = 0.6462$ with $S_{\rm Sr} = 1.83{\rm e}{-11}$. The low value of the two-sided significance confirms the above trend. This indicates that in flare-associated CMEs, faster CMEs tend to be accompanied by more intense flares.

4. Summary

With a sample of 86 flare-CMEs initiating in 55 active regions near the central meridian, we studied the properties of the longitudinal magnetic field of flare-CME productive active regions and their statistic correlations with CME speed. Four measures, tilt angle (*Tilt*), total flux (Ft), length of the strong-field and strong-gradient on the main neutral line (*Lsg*) and effective distance ($d_{\rm E}$), are used to quantify the magnetic properties. The main results are as follows:

(1) For CMEs initiating in active regions, fast CMEs tend to initiate in active regions with large Ft or large $d_{\rm E}$.

(2) In flare-associated CMEs initiating in active regions, faster CMEs tend to be accompanied by more intense flares.

(3) The parameters $d_{\rm E}$, *Lsg* and Ft correlate well with one another, especially Ft and *Lsg*.

(4) The occurrence of 11 slow CMEs and 1 fast CME in β type regions with *Lsg* far below the threshold reminds us of some exceptions to be considered when the *Lsg* with the threshold is used to predict CME productivity of active regions.

Acknowledgements. The authors are indebted to the anonymous referee for her/his insightful comments and suggestions that significantly improved the original manuscript. The authors would like to thank the SOHO team for providing their wonderful data. One of the authors (Juan Guo) thanks Dr. Jing Li for her discussions and good suggestions. This work is supported by the NSFC projects with 10233050, 10228307, 10311120115 and 10473016, the BRPC projects with TG2000078401, and 2006CB806301.

References

Canfield, R. C., Hudson, H. S., & McKenzie, D. E. 1999, Geophys. Res. Lett., 26, 627
Chae, J., Wang, H., Qiu, J., et al. 2001, ApJ, 560, 476
Chumak, O. V., & Chumak, Z. 1987, Kinematics and Physics of HeavenlyBodies, Kiev Naukova Dumka (in Russian), 3, 7
Falconer, D. A. 2001, J. Geophys. Res., 106, 25185
Falconer, D. A., Moore, R. L., Porter, J. G., & Gary, G. A. 1997, ApJ, 482, 519
Falconer, D. A., Moore, R. L., & Gary, G. A. 2003, J. Geophys. Res., 108, SSH11
Giovanelli, R. G. 1939, ApJ, 89, 555
Guo, J., Zhang, H. Q., Chumak, O. V., & Liu, Y. 2006, Sol. Phys., 237, 25
Hagyard, M. J. 1988, Sol. Phys., 115, 107
Hagyard, M.J., & Rabin, D. M. 1986, Adv. Space Res., 6, 7
Hahn, M., Gaard, S., Jibben, P., Canfield, R. C., & Nandy, D. 2005, ApJ, 629, 1135
Holder, Z. A., Canfield, R. C., McMullen, R. A., et al. 2004, ApJ, 611, 1149
Liu, J. H., & Zhang, H. Q. 2006, Sol. Phys., 234, 21
McIntosh, P. S. 1990, Sol. Phys., 125, 251
Moon, Y.-J., Choe, G. S., Wang, H. M., et al. 2002, ApJ, 581, 694
Moon, Y. J., Cho, K. S., Dryer, M., et al. 2005, ApJ, 624, 414
Moore, R. L., & LaBonte, B. J. 1980, Solar Interplanet. Dyn., 91, 207
Moore, R. L., Schmeider, B., Hathaway, D. H., & Tarbel, T. D. 1997, Sol. Phys., 176, 153
Moore, R. L., Sterling, A. C., Hudson, H. S., & Lemen, J. R. 2001, ApJ, 552, 833
Qiu, J., & Yurchyshyn, V. B. 2005, ApJ, 634, L121
Schmieder, B. 2005, IAUS, 226, 149
Subramanian, P., & Dere, K. D. 2001, ApJ, 561, 372
Tian, L. R., & Liu, Y. 2003, A&A, 406, 337
Tian, L. R., Bao, S. D., Zhang, H. Q., & Wang, H. N. 2001, A&A, 374, 294
Tian, L. R., Liu, Y., & Wang, J. X. 2002, Sol. Phys., 209, 361
Wang, H. M., Song, H., Yurchyshyn, V., et al. 2006, Chin. J. Astron. Astrophys., in press
Zhang, H. Q. 2001, ApJ, 557, L71
Zhang, H. Q. 2006, Advances in Geosciences: Solar Terrestrial, ed. M. Duldig, 2, 83
Zhang, H. Q., Ai, G. X., Yan, X., Li, W., & Liu, Y. 1994, ApJ, 423, 828
Zhou, G. P., Wang, J. X., & Cao, Z. L. 2003, A&A, 397, 1057
Zirin, H. 1988, Astrophysics of the Sun (Cambridge Unive. Press)
Zirin, H., & Liggett, M. A. 1987, Sol. Phys., 113, 267

Online Material

Table 1. Physical characteristics of the 86 CMEs.

Date	Time[a]	V^b (km s^{-1})	Flare Start	X-ray Class	Position (deg)	AR No.	Mag. Class	*Tilt* (deg)	*Ft* (10^{21} Mx)	d_E	*Lsg* (arcsec)
1997 Apr. 07	14:27	878	13:50	C6.8	S25E16	8027	β	−7.09	2.81	0.88	7 ⋆
1997 Oct. 21	18:03	523	17:00	C3.3	N17E05	8097	β	−156.88	4.64	0.46	0 ⋆
1997 Nov. 03	11:11	352	09:13	M1.4	S20W15	8100	$\beta\gamma\delta$	24.47	20.84	0.93	321
1997 Nov. 04	06:10	785	05:52	X2.1	S14W33	8100	$\beta\gamma\delta$	23.72	24.95	0.96	426
1998 Apr. 29	16:58	1374	16:06	M6.8	S18E20	8210	$\beta\gamma$	22.70	13.52	1.20	126
1998 May 01	23:40	585	21:40	C2.6	S19W05	8210	$\gamma\delta$	8.48	17.54	1.71	146
1998 May 02	05:31	542	04:48	C5.4	S19W10	8210	$\beta\gamma\delta$	7.00	17.96	1.70	142
1998 May 02	14:06	938	13:31	X1.1	S15W15	8210	$\beta\gamma\delta$	6.10	18.50	1.66	155
1998 May 03	22:02	649	21:12	M1.4	S13W34	8210	$\beta\gamma$	3.59	16.55	1.43	99
1998 Nov. 04	07:54	523	07:13	C1.6	N17E01	8375	$\beta\gamma$	40.63	16.98	1.29	153
1999 May 03	06:06	1584	05:36	M4.4	N17E32	8525	β	8.14	16.88	0.56	88
1999 May 10	05:50	920	05:24	M2.5	N16E19	8539	β	38.68	3.82	0.70	18 ⋆
1999 Aug. 07	23:50	283	23:04	C3.9	S28E03	8657	β	−0.35	6.72	0.74	60
1999 Aug. 17	13:31	776	12:47	C2.6	N22E34	8668	β	7.50	9.58	1.07	99
1999 Aug. 28	18:26	426	17:52	X1.1	S26W14	8674	$\beta\gamma\delta$	−8.21	66.39	1.02	692
1999 Sep. 01	02:30	253	23:56[c]	C2.7	N08W08	8677	β	4.64	3.25	0.54	5 ⋆
1999 Sep. 13	17:31	444	16:38	C2.6	N16W03	8693	β	82.69	2.10	1.03	13 ⋆
1999 Sep. 13	09:30	898	08:05	C4.9	N22E10	8699	β	17.99	8.90	0.63	96
1999 Oct. 14	09:26	1250	08:58	X1.8	N12E37	8731	$\beta\gamma\delta$	11.42	22.73	1.56	212
1999 Nov. 26	17:30	409	17:40	C2.3	S12W10	8778	β	2.05	14.30	0.77	136
2000 Jan. 18	17:54	739	17:10	M3.9	S19E11	8831	β	31.06	20.16	0.82	77
2000 Jan. 28	20:12	429	19:45	C4.7	S31W17	8841	β	12.99	6.19	0.57	56
2000 Feb. 09	19:54	910	19:26	C7.4	S14W40	8853	β	−31.46	5.10	0.61	0 ⋆
2000 Feb. 08	09:30	1079	08:43	M1.3	N25E26	8858	$\beta\gamma$	−141.07	9.20	2.95	200
2000 Feb. 12	04:31	1107	04:10	M1.7	N26E23	8858	$\beta\gamma$	−38.72	4.74	1.77	121
2000 Feb. 17	20:06	728	18:45	M2.5	S25W16	8869	$\beta\gamma$	−12.46	8.61	1.04	87
2000 Feb. 17	21:30	728	20:19	M1.3	S29E07	8872	β	32.46	6.15	0.59	6 ⋆
2000 Apr. 10	00:30	409	23:29[c]	M3.1	S14E01	8948	$\beta\gamma\delta$	99.52	13.80	4.03	327
2000 May 10	20:06	641	19:32	C8.7	N14E20	8990	β	20.58	7.68	0.66	133
2000 Jun. 02	10:30	442	09:04	C2.4	N10E23	9028	β	52.29	1.93	0.49	4 ⋆
2000 Jun. 06	15:54	1119	12:06	X2.3	N20E18	9026	$\beta\gamma\delta$	2.77	35.41	1.41	135
2000 Jun. 07	16:30	842	15:04	X1.2	N23W03	9026	$\beta\gamma\delta$	2.98	33.28	1.34	109
2000 Jun. 10	17:08	1108	16:37	M5.2	N22W38	9026	β	4.41	23.24	1.22	0 ⋆
2000 Jul. 10	21:50	1352	21:05	M5.7	N17E27	9077	$\beta\gamma\delta$	−19.56	33.94	1.84	310
2000 Jul. 14	10:54	1674	10:03	X5.7	N22W07	9077	$\beta\gamma\delta$	−32.45	33.40	2.10	227
2000 Jul. 25	03:30	528	02:47	M8.0	N06W08	9097	$\beta\gamma$	−13.10	21.71	0.94	134
2000 Aug. 09	16:30	702	15:33	C2.3	N11E11	9114	$\beta\gamma$	17.79	14.10	0.60	85
2000 Sep. 01	06:30	427	05:42	C1.6	S20W18	9143	β	−22.84	7.55	0.70	2 ⋆
2000 Sep. 15	12:06	633	10:54	C9.5	N13E08	9165	$\beta\delta$	−73.30	15.12	1.96	147
2000 Sep. 15	15:26	481	14:31	M2.0	N12E07	9165	$\beta\delta$	–65.84	16.10	1.87	134
2000 Sep. 16	05:18	1215	04:07	M5.9	N14W07	9165	$\beta\gamma$	−65.05	15.49	1.88	133
2000 Oct. 02	03:50	525	02:47	C4.1	S09E07	9176	$\beta\gamma$	6.68	21.04	0.71	56
2000 Oct. 09	23:50	798	23:22	C6.7	N01W14	9182	β	2.20	10.05	0.55	112
2000 Nov. 23	23:54	690	23:18	M1.0	N22W03	9236	β	15.51	21.47	0.62	255
2000 Nov. 24	05:30	994	04:55	X2.0	N20W05	9236	$\beta\gamma$	14.60	22.00	0.65	295
2000 Nov. 24	15:30	1245	14:51	X2.3	N22W07	9236	$\beta\gamma$	13.57	23.49	0.71	335
2000 Nov. 24	22:06	1005	21:43	X1.8	N21W14	9236	$\beta\gamma$	12.72	24.52	0.71	383
2000 Nov. 25	09:30	675	09:06	M3.5	N18W24	9236	$\beta\gamma$	11.76	25.51	0.77	304
2000 Nov. 25	19:31	671	18:33	X1.9	N20W23	9236	$\beta\gamma$	11.80	25.36	0.78	331
2000 Nov. 26	03:30	495	02:47	M2.2	N19W30	9236	$\beta\gamma$	11.08	25.68	0.77	272
2000 Nov. 26	17:06	980	16:34	X4.0	N18W38	9236	$\beta\gamma$	10.34	25.42	0.81	244
2000 Dec. 18	11:50	510	11:03	C7.0	N15E01	9269	β	–0.81	5.76	0.79	24 ⋆
2001 Jan. 10	00:54	823	00:34	C5.9	N13E36	9306	$\beta\gamma$	19.52	6.89	0.88	131
2001 Jan. 20	19:32	839	18:40	M1.2	S07E40	9313	$\beta\gamma$	3.57	7.53	2.44	204
2001 Mar. 24	20:50	906	19:37	M1.7	N15E22	9390	β	−4.80	11.05	0.91	99
2001 Mar. 28	12:50	519	11:21	M4.3	N18E02	9393	$\beta\gamma\delta$	−8.68	58.92	3.66	640
2001 Mar. 28	19:27	258	18:58	M1.5	N14W05	9393	$\beta\gamma\delta$	−7.09	60.38	3.46	655
2001 Mar. 29	00:26	526	23:25[c]	M2.1	N17W04	9393	$\beta\gamma\delta$	−5.60	61.10	3.35	660

Table 1. continued.

Date	Time[a]	V^b (km s^{-1})	Flare Start	X-ray Class	Position (deg)	AR No.	Mag. Class	*Tilt* (deg)	*Ft* (10^{21} Mx)	d_E	*Lsg* (arcsec)
2001 Mar. 29	10:26	942	09:57	X1.7	N17W18	9393	$\beta\gamma\delta$	−3.26	61.75	2.93	660
2001 Mar. 29	14:26	509	14:09	M1.6	N16W15	9393	$\beta\gamma\delta$	−4.42	61.45	2.86	700
2001 Apr. 06	19:30	1270	19:10	X5.6	S24E31	9415	$\beta\gamma$	−64.83	28.54	3.31	324
2001 Apr. 09	15:54	1192	15:20	M7.9	S21W04	9415	$\beta\gamma\delta$	−19.24	30.48	2.35	284
2001 Apr. 10	05:30	2241	05:06	X2.3	S23W09	9415	$\beta\gamma\delta$	−9.24	29.23	2.31	292
2001 Apr. 11	13:32	1103	12:56	M2.3	S22W27	9415	$\beta\gamma\delta$	−10.89	26.83	2.07	234
2001 Aug. 25	16:50	1433	16:23	X5.3	S17E34	9591	$\beta\gamma\delta$	−4.73	39.82	1.06	302
2001 Sep. 11	14:54	791	14:16	C3.2	N14E34	9615	β	−1.92	1.00	0.32	0 ⋆
2001 Sep. 17	08:54	1009	08:18	M1.5	S14E04	9616	$\beta\gamma$	3.48	23.53	0.68	45
2001 Sep. 24	10:31	2402	09:32	X2.6	S16E23	9632	$\beta\gamma\delta$	–0.79	22.40	1.48	207
2001 Oct. 19	01:27	558	00:47	X1.6	N16W18	9661	$\beta\gamma\delta$	34.44	33.46	1.35	300
2001 Oct. 19	16:50	901	16:13	X1.6	N15W29	9661	$\beta\gamma\delta$	35.71	31.03	1.31	326
2001 Oct. 22	15:06	1336	14:27	M6.7	S20E18	9672	$\beta\gamma\delta$	−162.00	22.81	1.59	176
2001 Oct. 25	15:26	1092	14:42	X1.3	S16W21	9672	$\beta\gamma\delta$	−160.03	27.51	1.92	170
2001 Nov. 01	22:30	453	21:38	M1.1	N12W23	9682	$\beta\gamma\delta$	16.39	40.02	1.12	327
2001 Nov. 04	16:03	1810	16:03	X1.0	N06W18	9684	$\beta\gamma\delta$	−9.94	23.16	1.24	126
2001 Nov. 17	05:30	1379	04:48	M2.8	S13E42	9704	β	–132.51	18.86	1.72	84
2001 Nov. 22	23:30	1437	22:09	M9.9	S15W34	9704	$\beta\gamma\delta$	−136.86	24.83	1.98	371
2001 Nov. 28	17:30	500	16:32	M6.9	N04E15	9715	$\beta\gamma\delta$	18.48	26.60	1.04	185
2001 Dec. 11	08:30	804	08:02	X2.8	N16E41	9733	$\beta\gamma$	17.66	28.67	0.92	202
2001 Dec. 13	14:54	864	14:24	X6.2	N16E09	9733	$\beta\gamma$	18.14	33.22	0.93	165
2002 Jul. 15	20:30	1151	19:50	X3.0	N19W01	10030	$\beta\gamma\delta$	14.73	41.86	0.96	397
2002 Aug. 16	12:30	1459	11:32	M5.2	S14E20	10069	$\beta\gamma\delta$	−30.85	51.05	1.99	642
2003 Oct. 28	11:30	2459	10:01	X17.2	S17E04	10486	$\beta\gamma\delta$	23.94	66.13	4.67	915
2003 Oct. 29	20:54	2029	20:37	X10	S15W02	10486	$\beta\gamma\delta$	32.73	66.87	3.82	877
2005 Jan. 15	06:30	2049	05:56	M8.6	N11E06	10720	$\beta\delta$	50.18	49.42	1.98	355
2005 Jan. 15	23:06	2861	21:54	X2.6	N14W08	10720	$\beta\delta$	54.88	41.72	2.34	394
2005 Jan. 17	09:54	2547	06:59	X3.8	N13W27	10720	$\beta\delta$	58.06	43.64	3.55	406

[a] Indicates the first appearance time in the LASCO C2 field of view.
[b] Indicates the representative speed of the linear fit in the LASCO C2 and C3 fields of view.
[c] Indicates the time on the day prior to the date given in the first column of the table.
⋆ Indicates the CME-productive active region with a *Lsg* below the threshold of 50 arcsec.